J Mater Sci (2011) 46:846–854
DOI 10.1007/s10853-010-4827-3

Nitrogen surface enrichment of austenitic stainless steel ISO 5832-1

R. F. Reis · A. M. Maliska · P. C. Borges

Received: 1 February 2010 / Accepted: 13 August 2010 / Published online: 27 August 2010

Abstract Austenitic stainless steels, although highly resistant to general corrosion, are susceptible to localized pitting or crevice corrosion. Corrosion resistance and mechanical properties could be enhanced by adding nitrogen to the alloy in solid solution. The methods currently in use involve fusion and solidification of the material, which may often be a deterrent, from the cost–benefit analysis stand point. In this article, the solution heat treatment after plasma nitriding (SHTPN) is presented as a new method to increase the surface nitrogen content in the solid state. The results obtained demonstrated the efficiency of this technique, by which the achieved thickness of the nitrided steel reaches up to 200 μm with 0.45 wt% of nitrogen.

Introduction

Stainless steels first appeared around 1910, heralding a significant technological breakthrough, due to their wide range of applications because of their amazing corrosion resistance. Further nitrogen has been added to these steels in order to improve mechanical resistance. Many researches describe several benefits of nitrogen addition to stainless steels, including enhanced resistance to corrosion, creep and fatigue, as well as higher yield and tensile strength [1–14].

In spite of that the most advantageous effects of adding nitrogen to stainless steels are related to its presence in solid solution [3]. Precipitation of chromium nitrides (CrNs), for instance, negatively affects corrosion resistance [1, 5, 6].

Several processes have been attempted for the addition of nitrogen in solid solution to stainless steels, the most common are plasma nitriding (PN) at low temperatures [7–11] and ion implantation [12, 13]. Recently, a high temperature gas nitriding (HTGN) or solution nitriding process was proposed as a means to add nitrogen to stainless steels [14, 15].

The thermodynamic tendency for nitride formation (M_xN_y) by PN can be lowered by working below 773 K. It is in such condition, that a phase termed expanded austenite (γ_N) or phase "S" occurs, which means that a nitrogen solid solution is created within the austenitic phase [6, 16]. This phase presents good corrosion resistance, although there are limitations due to the subsequent formation of extremely thin γ_N [6, 16, 17] surface layers.

Plasma immersion ion implantation (PIII) is another technique used to obtain high-nitrogen layers in stainless steel. Abreu et al. [12] studied the effect of incorporating nitrogen with an acceleration voltage of 150 kV and a saturation dose of 4×10^{17} ions/cm^2 on AISI 304L stainless steel. The implanted N^+ ions roughly penetrate up to 140 nm, although the maximum concentration is located at about 70 nm. The electrochemical behavior clearly reveals an improvement in the corrosion resistance, in the alkaline and chloride-containing media, for the implanted specimens. Ma et al. [13] applied the elevated temperature PIII

R. F. Reis · P. C. Borges (✉)
Federal University of Technology - Paraná, GrMaTS, DAMEC, UTFPR, Curitiba, PR 80230-901, Brazil
e-mail: pborges@utfpr.edu.br

R. F. Reis
e-mail: ricardo@utfpr.edu.br

A. M. Maliska
Federal University of Santa Catarina, LABMAT, EMC, UFSC, Florianópolis, SC 88040-900, Brazil
e-mail: ana@materiais.ufsc.br

technique, which combines the conventional ion implantation and diffusion, culminating in a change in the element distribution and microstructure in the implanted layer. By using this process, the resulting layer can reach a thickness of about 2 μm, which is approximately one order of magnitude thicker than the layer implanted at room temperature.

The HTGN method promotes the superficial enrichment of nitrogen in stainless steel, by employing a high-temperature thermochemical treatment, usually between 1,273 and 1,473 K, in a N_2 atmosphere. After the treatment, between 6 and 24 h, the nitrogen-enriched layers range from 0.5 to 3 mm [14]. In 1994, Berns patented a similar treatment (solution nitriding) attempting to obtain austenitic layers with high-nitrogen content, in different stainless steels [18].

The high temperatures and lengthy treatment used in HTGN result in formation of columnar coarse grains. However, for higher treatment temperatures, secondary grain growth could occur, depending on the material [14].

This study presents a two-stage route for surface nitrogen enrichment, called solution heat treatment after plasma nitriding (SHTPN). This treatment takes place in two steps: first, PN at high temperatures (above 873 K) is carried out, to produce thick nitrided layers, followed by the second step, where the material undergoes a solution heat treatment (SHT), aiming the diffusion of nitrogen and the consequent formation of a nitrogen-rich, precipitate-free, and thick nitrided layer. The method proposed here (SHTPN) aims to produce nitrogen-enriched layers thicker than those obtained by PN at low temperatures and PIII, and in reduced times comparing to HTGN technique.

Materials and methods

Cylindrical specimens, 15.0 mm in height, were obtained from a bar with 15.8 mm in diameter. Twelve specimens were prepared. After cutting the samples with appropriate cutoff wheel, they were ground with emery paper, and polished with 1 μm alumina suspension. ISO 5832-1 stainless steel was the material chosen in this research. Its composition is shown in Table 1. The starting microstructure of the steel was fully austenitic and its hardness 210 HV.

For the plasma treatment, samples were ultrasonically cleaned for 1 h, in ethanol.

Table 1 Nominal chemical composition of ISO 5832-1 stainless steel (wt%)

C	Mn	Si	Cr	Ni	Mo	N	Fe
0.017	1.750	0.350	17.800	14.300	2.760	0.077	Balance

Table 2 Parameters of the plasma nitriding treatment (PN)

Parameter	Sputtering cleaning	Plasma nitriding	
Temperature T (K)	673	903	1,023
Pulse duration T_{on} (μs)	550–650	700–850	750–850
Pulse pause T_{off} (μs)	250–400	400–500	150–200
Peak voltage U (V)	400	500	500
Total pressure P (Pa)	799.93	1,333	1,333
Time t (h)	1	3	3
Treatment gas	H_2	90% N_2 + 10% H_2	90% N_2 + 10% H_2

The samples were plasma nitrided in a pulsed DC glow discharge, in two consecutive stages. The first stage corresponded to sample cleaning by cathodic sputtering, and the second to the PN process itself.

The cleaning sputtering was carried out to remove the oxides comprising the external passive layer, which, as mentioned, is a characteristic of stainless steels. This cleaning stage was conducted only with hydrogen for 1 h, under the pressure of 799.93 Pa (6.0 Torr), and at 673 K. The nitriding process was performed under the pressure of 1,333 Pa (10 Torr), in a controlled atmosphere of 90% N_2 + 10% H_2. Specimens were separated into two groups for the nitriding process, one group was nitrided at 903 K and the other at 1,023 K. The nitriding time was 3 h for both groups. Finally, the samples were cooled to 573 K by forced convection in the same gas mixture, and then cooled under vacuum to room temperature. Table 2 summarizes the main parameters used in this processing step.

In the SHT step, commercial salt baths composed of barium chloride, boron chloride, and magnesium salts (tec 1080—TecFar®) were used. The treatment temperature was 1,473 K. For samples nitrided at 903 K the treatment time was 30 min, and for those nitrided at 1,023 K, it was 45 min. The choice of temperatures and duration of the SHT were based on the results published by Reis [2]. In this study, solution treatments were conducted at 1,313, 1,393, and 1,473 K and times of 15, 30, 45, and 60 min for each of them. In all the analyzed conditions, the parameters employed in the SHT were chosen to ensure the dissolution of nitrides and hinder grain growth.

The SHT process could be performed in a vacuum furnace. However, the salt bath was chosen because of the versatility of this process, which allows the simultaneous treatment of several specimens, and removing them from the treatment at different treatment times.

After the processes described above, both the nitrided and the SHTPN samples were longitudinally cut and

mounted in resin. The cross-sections obtained were prepared with an adequate metallographic process to investigate the morphology, thickness, and microhardness profile of the resulting layers. The morphology evaluation of the nitrided layers was done using scanning electron microscopy (SEM) and energy-dispersive spectroscopy (EDS). In the SHTPN process, the samples were analyzed by optical microscopy to verify the treatment effectiveness. In both cases, electrolytic etching with aqueous solution of oxalic acid (10%) was employed. Thickness measurements of the nitrided layer were made with an image analyzer (Image Pro-Plus) attached to an optical microscope. Microhardness profile measurements (Vickers indenter, 50 gf) were conducted, both for the nitrided case and the matrix. Using a Philips diffractometer with Cu $K\alpha$ radiation, 2θ-scan step of 0.05°, and range from 20 to 120°, X-ray diffraction (XRD) analysis was performed for phase identification.

The nitrogen content on surface of the SHTPN samples was measured by wavelength dispersive spectrometry (WDS) microanalysis in the longitudinal section. Wavelength dispersive analyses were carried out in an Oxford WDX600 spectrometer with take-off angle of 35°, coupled to a Cambridge Stereoscan 440 SEM equipped with LaB6 emission source operating at 10 kV. Nitrogen was measured using synthetic LSM60 crystal. The setup procedure for quantitative analysis included the following steps:

1. Electron beam stabilization monitored by repetitive measurements of beam current in a Faraday cup. The beam current was fixed in 100 nA for all the measurements by controlling the condenser aperture;
2. Preliminary X-ray acquisition from standard, which was used to define the peak acquisition window and the background level;
3. Acquisition of X-ray spectra of standard sample, which was an austenitic high-nitrogen stainless steel (18 wt% Cr–15 wt% Mn–0.39 wt% N), solubilized at 1,200 °C during 6 h and water quenched; and
4. Acquisition of X-ray spectra of SHTPN samples.

Measurements were performed alongside the hardness profile indentations of the modified layer. Magnetic measurement of SHTPN samples was done using a ferritoscope. The equipment detection limit is 0.1% of ferrite.

Results and discussion

Plasma nitriding

Figures 1 and 2 show the structure of the layers obtained by PN at 903 and 1,023 K, respectively. At 903 K, the layer was essentially composed of nitrided case. However, nitriding at 1,023 K, showed a "diffusion layer" (zone B),

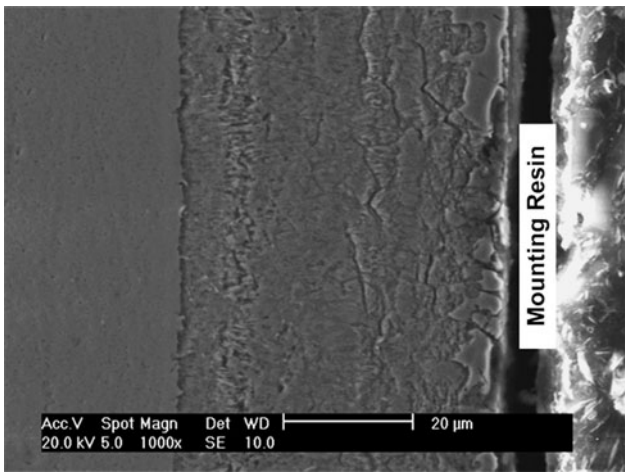

Fig. 1 SEM micrograph of stainless steel ISO 5832-1 plasma nitrided at 903 K. Electrolytic attack: oxalic acid 10%

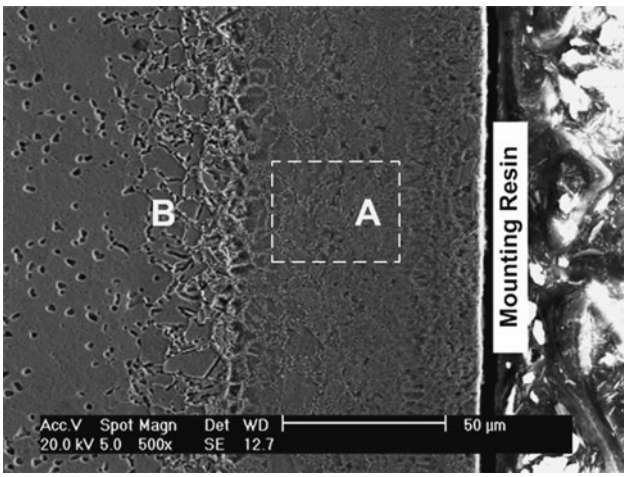

Fig. 2 SEM micrograph of stainless steel ISO 5832-1 plasma nitrided at 1,023 K. Zone A: nitrided case and zone B: diffusion layer. Electrolytic attack: oxalic acid 10%

in addition to the nitrided case (zone A), which is related to the grain boundary precipitates formed due to the high nitriding temperature. In both micrographs, microstructural differences are observed along the thickness of the nitrided case. This differences were studied in the earlier papers [2, 19–21]. Table 3 shows some results for the same nitriding conditions employed in this article. As can be seen (Table 3), an increase in the depth decreases the amount of nitrogen-rich phases or the appearance of martensite (α') and/or gamma iron (γ). This occurs for the samples nitrided at both temperatures (903 and 1,023 K). For those samples nitrided at 903 K, a reduction in the amount of CrN formed was observed, and even more nitrogen-poor phases for higher depths [20]. The XRD analysis on the surface and at the depth of 35 µm revealed the disappearing of γ' phase (Fe_4N) and appearing of

Table 3 Phases on nitrided layers [2, 19–21]

Treatment temperature (K)	Depth (μm)	Phases
903	Surface	CrN, γ' (Fe_4N)
	35	CrN, γ_N
	50	CrN, γ
1,023	Surface	CrN, γ, α'
	50	CrN, γ, α'
	90	γ

expanded austenite phase (γ_N). Comparing the results on 35 and 50 μm, it can be verified that the expanded austenite (γ_N) has been substituted by austenite (γ). This sequence of phases changing makes evident the reduction of nitrogen as distance from surface increases. For the samples nitrided at 1,023 K, it can be observed a reduction in CrN content from the surface to the core, as well as an increase of γ phase [21]. It was noticed that the martensite (α') and iron austenite (γ) phases appear not only on the surface, but also at 50 μm. When the XRD was performed at the depth of 90 μm, which corresponds to the diffusion layer, it was not possible to detect the chromium precipitates. As can be seen in Fig. 3, as depth increases, precipitates morphology changes from a discontinuous (lamellar shape) to a continuous precipitation (needles forming angles of about 60°). These morphologies were reported in other studies [22–24]. In fact, the discontinuous precipitation is associated with the nitrogen richer regions, while the continuous precipitation is linked to the nitrogen-poor regions [22]. Therefore, the microstructural differences observed can be explained by the nitrogen distribution across the layer, which decreases from the surface to the core, leading to the formation of different phases, as well as causing the morphology change in CrN precipitates from discontinuous (lamellar) to continuous [2, 19–21].

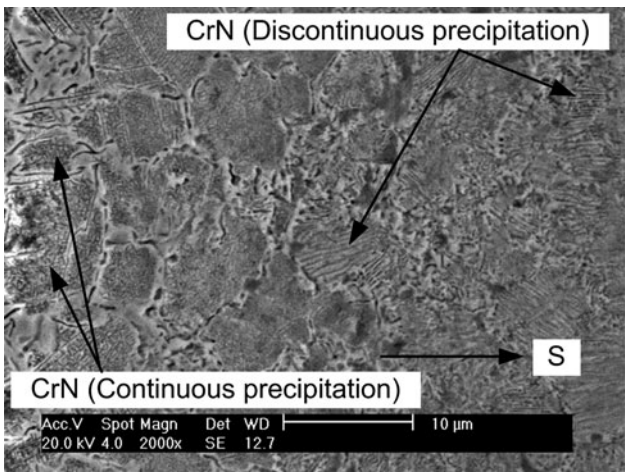

Fig. 3 Detail of zone A indicated in Fig. 2 (S—indicates the surface direction)

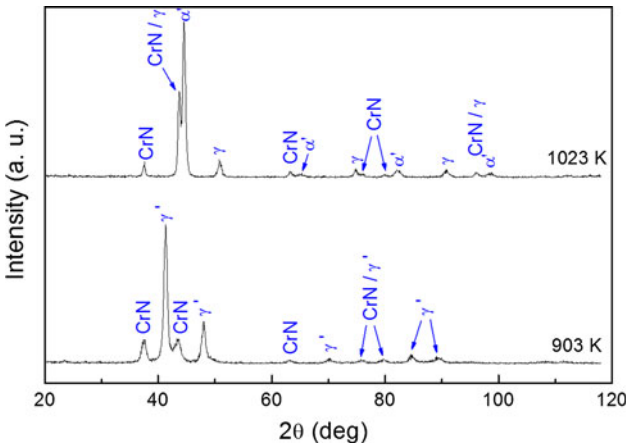

Fig. 4 X-ray diffraction patterns of samples PN at 903 and 1,023 K

The identification of phases present on the surface of the nitrided samples at 903 and 1,023 K was performed by XRD, as shown in the diffractograms of Fig. 4.

As could be seen in Table 3 and Fig. 4, besides the non-formation of γ' (Fe_4N), the nitriding at 1,023 K caused the formation of α' (martensite) and γ (austenite) phases in the samples. This behavior has been already reported and discussed in earlier papers [19–21].

Reis et al. [19] measured the nitrogen content on surface of similar stainless steel (AISI 316L) plasma nitrided (PN) at 743, 923, 1,023, 1,123, and 1,323 K, by X-ray photoelectron spectroscopy (XPS), and verified that the nitrogen content decreases when the temperature increases.

The nitrogen equilibrium on the steel surface depends on the temperature, pressure, atmosphere, species energy, and alloy composition. Lopez et al. [25] using ThermoCalc®, calculated phase diagram for AISI 304 in equilibrium with gaseous nitrogen at different pressures. It can be verified that the increase in temperature causes a reduction of the nitrogen chemical potential on the surface of the steel. Therefore, by increasing temperature from 903 to 1,023 K a thicker layer is obtained, influenced by diffusion, but it presents lower surface nitrogen content. This explains the existence of the γ phase in the samples nitrided at 1,023 K, which is related to the original material structure. For both processing temperatures, the presence of CrN was expected, once the employed temperatures were higher than 773 K [1, 5, 6].

At a temperature of 1,023 K, the formation of α' (martensite) from the Fe–Ni system, also reported in other studies, was verified and it was found to be linked to the chromium loss by the matrix due to CrN precipitation [17, 21, 26]. EDS analysis on the region of discontinuous precipitates (lamellar shape) exhibited chromium contents of 3.5 wt% in α' (martensite) and 65.3 wt% in CrN precipitate. As an attempt to understand the formation of α' (martensite) calculations of Cr_{eq} (chromium equivalent) and Ni_{eq} (nickel equivalent) were proceeded, according to

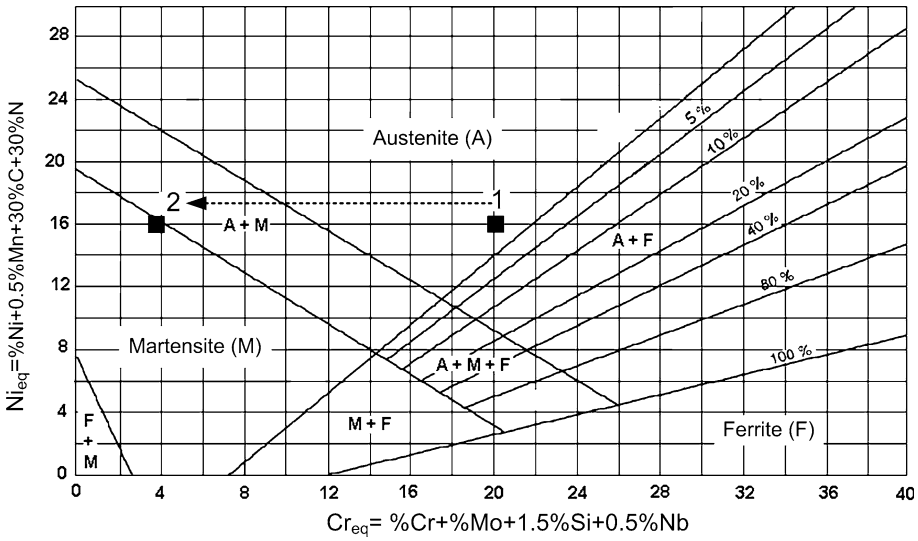

Fig. 5 Compositional positions of material on starting condition (1) and on depleted Cr region (2) shown in Schaeffler-type diagram using DeLong's formula

DeLong's equations [27]. The results for the original steel composition of the steel and for the chromium-depleted region were plotted in a Schaeffler-type diagram (Fig. 5), as Point 1 and Point 2, respectively. According to the diagram it is clear that the reduction of chromium content in the matrix to 3.5 wt% leads the α' (martensite) formation.

For the specimens nitrided at 903 K, although the amount of CrN formed was higher than for those nitrided at 1,023 K, as can be observed by the intensity of the peak where CrN appears alone ($2\theta = 37.54$), no α' phase formation was observed. This is justified by the higher amount of nitrogen in this condition [28], which increases Ni_{eq} and consequently stabilizes austenite, suppressing the formation of α' (martensite).

The formation of CrNs is associated with more negative Gibbs energies, and as temperature increases the Gibbs energy become more positive for CrNs as can be seen on Ellingham Diagram [29]. In other words, the more temperature increases, the less stable CrN becomes, which agrees with the reduction of CrN as nitriding temperature changed from 903 to 1,023 K.

The average thicknesses of the layers obtained for the temperatures used in the studies are listed in Table 4. By increasing the temperature it can be observed an increase in the nitrided layer thickness. Reis [2] verified that this growth is ruled by diffusion for a temperature range from 903 to 1,143 K.

Table 4 Nitrided layer thickness versus nitriding temperature

Temperature (K)	Nitrided case (μm)	Nitrided (nitrided case + diffusion) (μm)
903	50 ± 2	50 ± 2
1,023	78 ± 2	102 ± 3

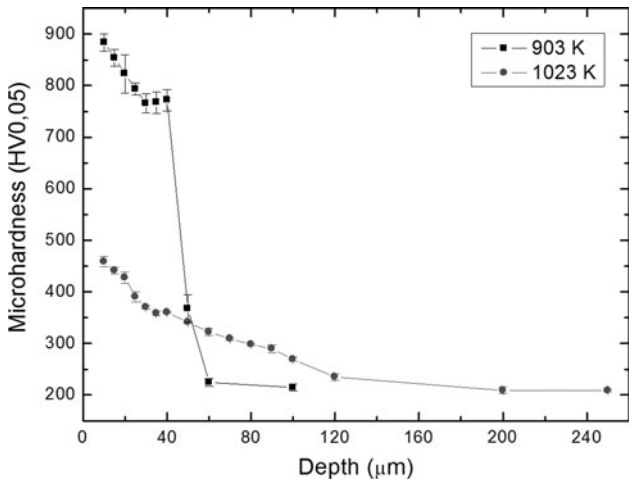

Fig. 6 Microhardness profile of samples PN at 903 and 1,023 K

Figure 6 illustrates the variation of Vickers microhardness HV0.05 as a function of depth for both PN treatments. The microhardness values are noted to be lower for the 1,023 K nitriding temperature, however, with an increase in the hardening depth. This result agrees with the previous discussion concerning the drop in the nitrogen content and its effects on the phases present in the nitrided layer. The layer obtained with nitriding at 1,023 K presents not only a lower amount of nitrides, compared to nitriding at 903 K, but also the formation of γ, which contribute to the noticeable hardness drop.

Another aspect already discussed in earlier papers [4, 19, 21] is related to an increase in the precipitate size in response to a temperature rise. This increases the average distance between the precipitates, which consequently facilitates the dislocation movement, also contributing to a hardness drop.

Solution heat treatment of plasma nitrided samples

As mentioned in "Materials and methods" section, the parameters employed in the SHT step were based on previous results [2]. Among all the temperature and times combinations employed (1,313, 1,393 and 1,473 K and 15, 30, 45, and 60 min), only those presenting the complete solution associated to a lower grain growth for the nitriding conditions are presented in this article.

The time required for the complete dissolution of the nitrided layer on SHT processes was longer for samples nitrided at the higher temperature (1,023 K). This effect can be explained by the higher nitriding temperature, resulting in larger CrN precipitates (see Figs. 1 and 2), and thicker nitrided case (see Table 4). Therefore, more time was necessary to completely dissolve these precipitates. Even at greater magnification, it was not possible to see the lamellar shape corresponding to discontinuous precipitation in the samples nitrided at 903 K (Fig. 1). For samples nitride at 1,023 K this morphology is characterized by the coarse precipitates shown in Fig. 2.

Figure 7 presents the microstructure resulting from the SHT results of a specimen nitrided at 903 K, which indicates a precipitate-free structure. To verify the possible existence of chromium-based precipitates, a long duration of electrolytic attack was conducted on the surface. As shown in Fig. 8, no intergranular etching was observed at the grain boundary. The XRD analyses presented in Fig. 9 indicated only the presence of austenite, while magnetic measurement using a ferritoscope did not reveal any presence of ferrite.

For the nitrided specimens at 1,023 K and 45 min of SHT a similar analysis was proceeded, and it was evidenced the success of this processing step, in other words,

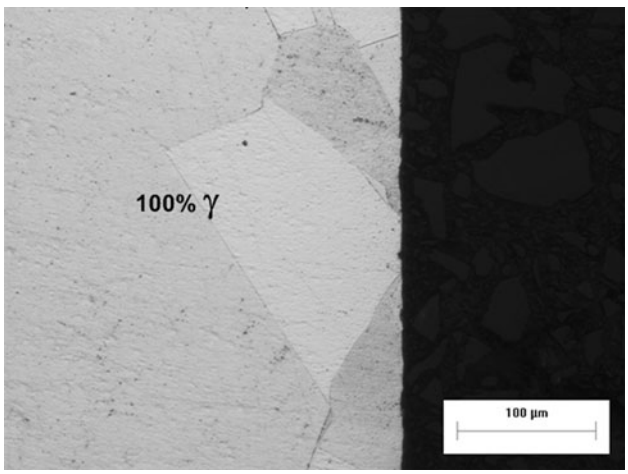

Fig. 7 Microstructure of sample PN at 903 K/SHT for 30 min (SHTPN). Electrolytic attack: oxalic acid 10%

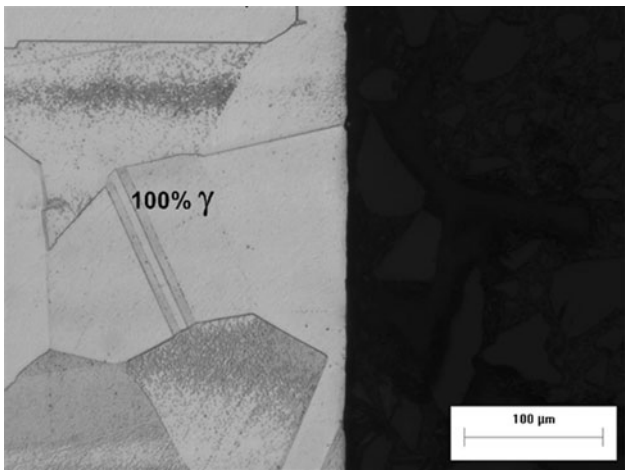

Fig. 8 Microstructure of sample PN at 903 K/SHT for 30 min (SHTPN). Long time electrolytic attack: oxalic acid 10%

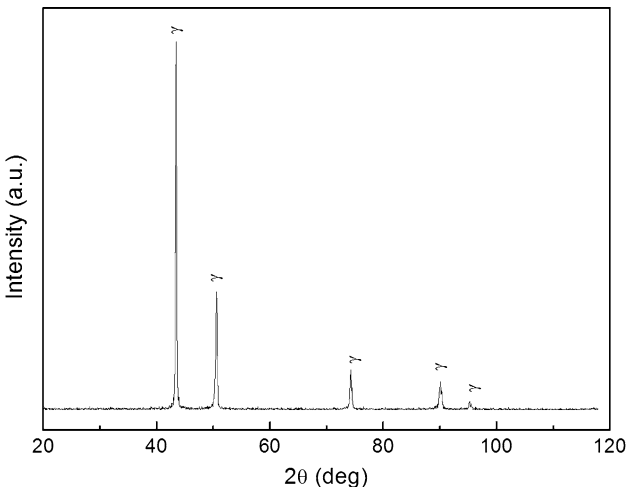

Fig. 9 X-ray diffraction pattern of samples PN at 903 K/SHT for 30 min

the achievement of a precipitate free, 100% austenitic structure.

The dissolution of the nitrides during the SHTPN is promoted by the increase in nitrogen solubility in austenite and reduced nitride stability with the temperature increase.

Following the nitrided layer dissolution and the nitrogen diffusion to the core of the specimens, the analysis of surface nitrogen content in solid solution should indicate values higher than in the initial condition, which leads to a higher surface hardness.

Figures 10 and 11 present the hardness profiles for the specimens after SHTPN treatment, compared with the hardness obtained after the nitriding (PN) and the initial specimen hardness. The analysis of these figures allows verifying the strong hardening effect of nitrogen in solid solution. Even occurring a considerable increase of the average grain diameter of the nitrided samples, which was

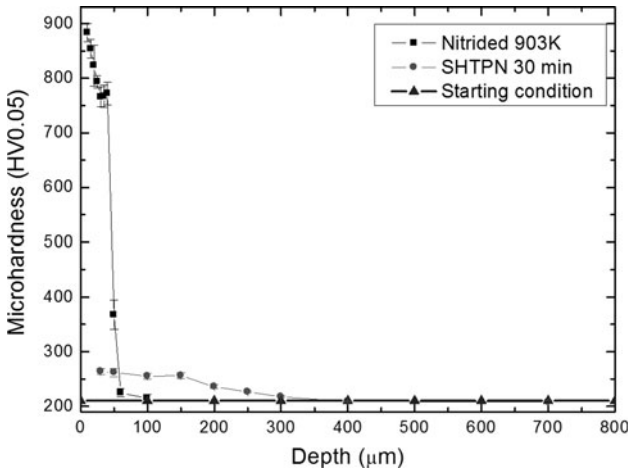

Fig. 10 Microhardness of starting condition; PN at 903 K and PN at 903 K/SHT for 30 min

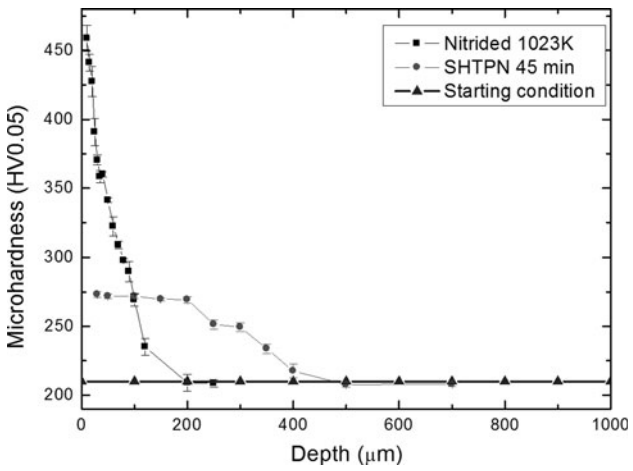

Fig. 11 Microhardness of starting condition; PN at 1,023 K and PN at 1,023 K/SHT for 30 min

7.72 ± 0.25 μm in the supply state and became 131 ± 8 μm in the samples processed by SHTPN for 30 min and 159 ± 9 μm in those processed by SHTPN for 45 min, the hardness after processing had a considerable increase. This way, it can be concluded that the effect of nitrogen in solid solution on the hardness overlaps the grain growth occurred in the process. As the grain diameter average obtained with the process is considerably higher, one can suggest that the material could go through other processes aiming a grain refining, as approached in other works [30, 31].

The hardness profile of the sample PN at 903 K and SHT for 30 min, shown in Fig. 10, indicates that hardness is almost constant up to depth of 150 μm. For the sample PN at 1,023 K and SHT for 45 min, the corresponding constant hardness reaches about 200 μm, as seen in Fig. 11,

Table 5 Nitrogen measurement (WDS) on treated samples (SHTPN)

Sample	Depth (μm)	% *N* (wt) Average/SD
PN 903 K	25	0.33/0.01
SHT 30 min	50	0.36/0.02
	100	0.27/0.03
PN 1,023 K	25	0.46/0.08
SHT 45 min	150	0.43/0.08

suggesting a quasi-homogeneous nitrogen distribution within the indicated depths. However, the regions affected by the nitrogen enrichment are approximately 300 and 400 μm deep, for the samples PN at 903 K and SHT 30 min, and PN at 1,023 K and SHT for 45 min, respectively.

In both samples the nitrogen content was measured by WDS, in the uniform hardness layer (UHL). Table 5 lists the measured values and their positions.

Table 6 summarizes the main results obtained after the SHT stage for both conditions used in PN.

The thickness and nitrogen content of the layers were observed to be higher in the plasma nitrided specimen at 1,023 K and SHT at 1,473 K for 45 min (see Table 6).

As discussed in the item 3.1 the samples nitrided at 1,023 K present surface nitrogen content lower than those nitrided at 903 K. On the other hand, this condition presents a thicker layer and consequently can present a higher total content of nitrogen incorporated during PN. This justifies that after SHT, samples nitrided at 1,023 K present more nitrogen content, as well as higher layer thickness.

For the alloy studied, an equilibrium diagram was obtained using Thermocalc® [32], a thermodynamic calculus software that helps to draw phase diagrams and evaluate the transformations of the systems studied.

The alloy diagram calculated using Thermocalc® indicates that the maximum nitrogen solubility at 1,473 K is 0.6 wt%, as illustrated in Fig. 12. This value was not exceeded, as verified by the measuring the total amount of nitrogen on the sample surface, after SHTPN, suggesting that all the nitrogen present is in solid solution within the austenite, as confirmed by microstructural analysis.

For those specimens nitrided at 903 K and SHT for 30 min, the microhardness profile (Fig. 10) was correlated with the amount of nitrogen obtained by WDS analysis (Table 5), for points at 25, 50, and 100 μm in depth. It was found a linear correlation between the amount of nitrogen and the hardness (Eq. 1). The purpose of this equation is to help in an estimative of nitrogen content to the used alloy. This equation does not consider the effect of other microstructural features such as the grain size and twinning. The sample used in the definition of the equation had a grain diameter average of 131 ± 8 μm.

Table 6 Obtained results for the treated samples (SHTPN)

Processing		Thickness of the nitrided case (μm)		% *N* (wt) (UHL)	% Ferrite
Plasma nitriding	Solution heat treatment	Total	UHL		
903 K	30 min	300	150	0.32 ± 0.04	0
1,023 K	45 min	400	200	0.45 ± 0.08	0

UHL uniform hardness layer

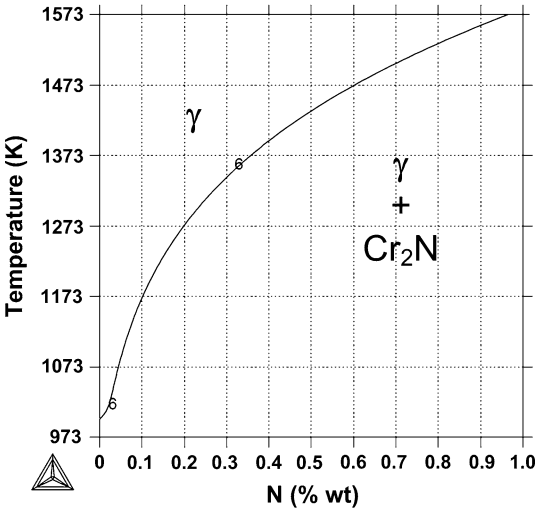

Fig. 12 Solubility limit of nitrogen in the austenite in relation to the nitrides precipitation for the steel ISO 5832-1

$$\%N = 0.0105\ \mathrm{HV} - 2.4116, \quad (1)$$

where *%N* denotes nitrogen content in weight, HV denotes Vickers microhardness.

The present article focuses exclusively on the SHTPN process. In stepfather works mechanical characterization and corrosion resistance of the processed materials will be conducted. However, based on the surface nitrogen content values reached and presented in Table 6, an increase in corrosion resistance can be deduced. This is based on the calculation of pitting resistance equivalent number (PREN) parameter, which provides a corrosion resistance estimative based on the chemical composition of the alloy. In the starting condition, according to the chemical composition presented in Table 1, this parameter has a value of 28.1. For the specimens nitrided at 903 K and SHT for 30 min, in which the nitrogen content increases from 0.077 to 0.32%, this value is 32.0, whereas for the specimens nitrided at 1,023 K and SHT for 45 min, in which the nitrogen content increases from 0.077 to 0.45%, it is 34.1. Berns and Siebert [33] studied the effect of solution nitriding on properties of stainless steels. This process produces a high-nitrogen case with a martensitic or austenitic microstructure depending on the grade of the stainless steels. The pitting potential of the high-nitrogen steels shows a slight shift to a higher potential which stands for an improved pitting resistance. These materials revealed a higher erosion resistance of the austenitic case with or without precipitates under severe working conditions. Borges and Rocha [34] studied the effect of SHTPN on the corrosion resistance of precipitation hardening stainless steel (AISI 15-5 PH) in a 3.5% NaCl aqueous solution. They concluded that the nitrogen content on the surface layer turns the sample surface into austenite, with traces of martensite. The thickness of these layers was 300, 320, and 430 μm for SHTPN at 1,373, 1,473, and 1,548 K, respectively. SHTPN was observed to improve the corrosion resistance for all conditions. The effect of nitrogen was to increase the pit nucleation potential.

Conclusions

- The results obtained in this study prove that increasing the surface nitrogen content of commercial steel using SHT after plasma nitrided—SHTPN is really possible. According to the proposed processing, a steel initially containing 0.077% in weight of nitrogen, can reach up to 0.32% at a depth of 150 μm, or up to 0.45%, at a depth of 200 μm, depending on the SHTPN parameters.
- The surface modification allows an increase on the PREN value indicating a possible increase in the pitting corrosion resistance.
- The nitrogen-enriched layers obtained by the proposed method (SHTPN) are thicker than those obtained by PN at low temperatures and PIII, and the processing times are shorter compared with the HTGN.
- The increase of the amount of solid solution nitrogen in the steel causes a linear variation in the microhardness value. The relationship between these two variables for the ISO 5832-1 steel can be estimated by Eq. 1, which may simplify further developments by requiring only hardness measures rather than a full WDS analysis in order to estimate nitrogen content, as a first approach, in similar conditions.

Acknowledgements The authors wish to thank Villares Metals for the donation of the material employed in the research and SOCIESC—SC for the salt bath solution heat treatment.

References

1. Fossati A, Borgioli F, Galvanetto E, Bacci T (2006) Corros Sci 48:1513
2. Reis RF (2007) Thesis (doctor degree), UTFPR, Curitiba
3. Gavriljuk VG, Berns H (1999) High nitrogen steels. Springer, Berlin
4. Borges PC, Martinelli AE, Franco CV (2004) Mater Corros 55:594
5. Liang W (2003) Appl Surf Sci 211:308
6. Borgioli F, Fossati A, Galvanetto E, Bacci T (2005) Surf Coat Technol 200:2474
7. Larisch B, Rusky BU, Spies HJ (1999) Surf Coat Technol 116–119:215
8. Liang W, Bin X, Zhiwei Y, Yaqin S (2000) Surf Coat Technol 130:304
9. Lin JF, Chen KW, Wei CC, Ai CF (2005) Surf Coat Technol 197:28
10. Xi Y, Liu D, Han D (2008) Surf Coat Technol 202:2577
11. Bernardelli EA, Borges PC, Fontana LC, Floriano JB (2010) Kovove Mater 48:105
12. Abreu CM, Cristóbal MJ, Merino P, Nóvoa XR, Pena G, Pérez MC (2008) Electrochim Acta 53:6000
13. Ma X, Jiang S, Sun Y, Tang G, Sun M (2007) Surf Coat Technol 201:6695
14. Garzón CM, Tschiptschin AP (2005) Rev Matér 10:502
15. Sung JH, Kong JH, Yoo DK, On HY, Lee DJ, Lee HW (2008) Mater Sci Eng A 489:38
16. Fossati A, Borgioli F, Galvanetto E, Bacci T (2006) Surf Coat Technol 200:3511
17. Gontijo LC, Machado R, Miola EJ, Casteletti LC, Alcântara NG, Nascente PAP (2006) Mater Sci Eng A431:315
18. Berns H (1994) Patent DE4333917, April 2
19. Reis RF, Schreiner WH, Borges PC (2006) Rev Bras Apl Vácuo 25:183
20. Reis RF, Maliska AM, Borges PC (2008) Rev Matér 13:304
21. Reis RF, Maliska AM, Borges PC (2007) Rev Brasil Apl Vácuo 26:205
22. Machado IF (1999) Thesis (doctor degree). EP-USP, São Paulo
23. Kikuchi M, Kajihara M, Choi S-K (1991) Mater Sci Eng A146:131
24. Vanderschaeve F, Taillard R, Foct J (1995) J Mater Sci 30:6035. doi:10.1007/BF01151525
25. López D, Falleiros NA, Tschiptschin AP (2007) Wear 263:347
26. Liang W, Juncai S, Xiaolei X (2001) Surf Coat Technol 145:31
27. DeLong WT, Ostrom GA, Szumachowski ER (1956) Weld J 35:521
28. American Society for Metals (1991) ASM handbook, vol 4. Ohio American Society for Metals, OH (Surface hardening steel, p 264)
29. Ellingham diagram web tool: http://www.engr.sjsu.edu/ellingham/
30. Tanaka M (1994) Z Metallkunde 85:446
31. Nakada N, Hirakawa N, Tsuschiyama T, Takaki S (2007) Scr Mater 57:153
32. Sundman B (1998) Thermocalc user's guide, version M. Royal Institute of Technology, Stockholm
33. Berns H, Siebert S (1996) High nitrogen austenitic cases in stainless steels, IJIS Inter., vol 36, no 7, p 927
34. Borges PC, Rocha LA, Kovove Mater (unpublished data)